Journal of Modern Optics

ISSN: 0950-0340 (Print) 1362-3044 (Online) Journal homepage: http://www.tandfonline.com/loi/tmop20

Ptychographical imaging with partially saturated diffraction patterns

XingChen Pan, Suhas P Veetil, Baosheng Wang, Cheng Liu & Jianqiang Zhu

To cite this article: XingChen Pan, Suhas P Veetil, Baosheng Wang, Cheng Liu & Jianqiang Zhu (2015) Ptychographical imaging with partially saturated diffraction patterns, Journal of Modern Optics, 62:15, 1270-1277, DOI: 10.1080/09500340.2015.1034207

To link to this article: http://dx.doi.org/10.1080/09500340.2015.1034207

Published online: 05 May 2015.

Journal of Modern Optics, 2015
Vol. 62, No. 15, 1270–1277, http://dx.doi.org/10.1080/09500340.2015.1034207

Ptychographical imaging with partially saturated diffraction patterns

XingChen Pan[a], Suhas P Veetil[b], Baosheng Wang[c], Cheng Liu[a]* and Jianqiang Zhu[a]

[a]*Shanghai Institute of Optics and Fine Mechanics, Chinese Academy of Sciences, Shanghai, China;* [b]*Department of Engineering Technology and Science, Higher Colleges of Technology, Fujairah, United Arab Emirates;* [c]*College of Sciences, Jiangnan University, Wuxi, China*

(*Received 27 November 2014; accepted 19 March 2015*)

In ptychographical imaging with X-ray or electron beam, the recorded speckle intensity pattern of far field diffraction was often saturated by the presence of strong zeroth-order which was undesirable. A beam-stop was widely used to block the area of strong central diffraction in the pattern. The image was then reconstructed by disregarding the diffraction constraints within that area where inaccuracies exists due to saturation or blocking of the beam. Though reconstructions were obtained in this way by omitting saturation regions, the rationale behind this method was not discussed in detail and its effect on the final image quality was not studied. The physics of this method was analyzed theoretically and experimentally in this study. The convolution effect between illumination and object functions was able to retrieve and bring back the information lost in the blocked or saturated area from its neighborhood. This was possible while the saturated or blocked area was not wider than the spectral width of illumination, and once it exceeds this minimum, the quality of reconstruction would degrade seriously. The theoretical model was verified by numerical simulations and experiments.

Keywords: phase measurement; phase retrieval; image reconstruction; coherence imaging

1. Introduction

In microscopic imaging with electron beam and X-ray, the spatial resolution that can be reached is mainly limited by the optics quality rather than by the diffraction limit. For example, due to the lack of high-quality optics, the highest spatial resolution reached with the electron microscope is only about 0.2 nm, which is much lower than the wavelength of 0.025 Å for 200 kV electron [1]. To circumvent the difficulty in getting high-quality optical elements, lensless imaging techniques including holography and coherent diffraction imaging (CDI) were developed to improve the spatial resolution without using high-quality optics [2]. The algorithm of CDI was firstly proposed in 1970s [3–5], and latterly developed by Gerchberg and Saxton [6], Fienup [7,8], and Nellist et al. [9] Owing to the simplicity in its setup and its lower requirement on the environment, CDI has received much attention and became quite successful in observing the sample with nanometer resolution [10–12]. However, it still suffers from disadvantages including stagnation, low convergence, and limited field of view [13–15]. To overcome these limitations, ptychographical iterative engine (PIE) algorithm was proposed [16] by combining the ideas of conventional ptychography and iterative phase retrieval. This proved to be a powerful technique to reconstruct the scattered wavefront by laterally shifting the illumination relative to the specimen. Making use of several diffraction patterns recorded by placing the incident beam at different positions, the complex transmission function of the specimen can be recovered in its amplitude and phase, and thus the structural information of specimen to be studied can be obtained. Compared to other CDI methods, PIE has wider field of view, faster computation convergence, and higher stability. With such merits, the PIE method has attracted much attention in recent years and has been successfully realized with visible light, hard X-rays, and electron beam [17–21]. Thibault introduced a probe retrieval into ptychography for scanning X-ray diffraction microscopy and this algorithm was named ePIE (extended ptychographical iterative engine) by Maiden [19], which could reconstruct the illumination probe and the sample simultaneously, and hence overcomes the difficulty of estimating the illumination in advance and enhances the practical use of PIE. Zhang [22] and Maiden [23] proposed the cross correlation algorithm and anneal arithmetic algorithm, respectively, to solve the problem of PIE in finding the correct positions of illumination probe relative to the sample being studied. This makes PIE algorithm to drop off the dependency of resolution on the accuracy of the scanning mechanism. However, in order to reach the spatial resolution determined by numerical aperture of the setup, the dynamic range of detector should be carefully considered in practical experiments. The sample

*Corresponding author. Email: chengliu@siom.ac.cn

studied with PIE technique is always weakly scattering and most part of the illumination beam is transmitted directly; almost without any change, and leaves a strong zero-order diffraction on the recording plane. Only a small portion of the illumination beam departs from its original direction and forms weak higher order diffractions on the recording plane. In most of the cases, the intensity of zero-order diffraction is hundreds or thousand times stronger than that of the higher order diffraction, which is the reason why a beam-stop is commonly used in X-ray and electronic imaging [24–26]. Due to the limited dynamic range of detector, it is difficult to simultaneously record the strong zero-order and weak higher order diffractions accurately. A practical approach adopted is to record the strong zero-order diffraction with shorter exposure time and the weak diffraction with longer exposure time and then combine them together properly to get whole diffraction pattern. Theoretically, the dynamic range of CCD camera can be increased infinitely in this way; however, since the data acquisition time becomes longer in this way, the stability requirement on environment and setup increases obviously. Another way is to disregard the inaccurate diffraction constraint within that area in the diffraction pattern due to either saturation or beam-stop [24–27]. The robustness of this method has been demonstrated using numerical simulations [28]. However, the rationale and underlying physics of this method are still not clearly known. This paper presents a detailed mathematical model to explain why clear reconstruction can be generated with partially saturated or blocked diffraction intensity in some cases and finds out the condition for this method to be adopted. It is found that only when the size of saturated or blocked area is kept within a minimum decided by the optical setup, the information lost by the saturation or beam-stop can be retrieved from its neighborhood, else no clear reconstruction can be generated with this method. The theoretical analysis is followed by numerical simulations and a series of experiments are conducted to demonstrate the feasibility of this study.

2. Theoretical analysis

According to the theory of Fresnel diffraction in Fourier optics, when an object $g(x,y)$ is illuminated by a light field $p(x,y)$, the diffraction of its exit wave after propagating a distance z could be described by Equation (1), where (x,y) and (u,v) represent the coordinates in the object domain and Fourier transform domain, and the operator notation * and *FFT* represent the convolution operator and Fourier transform, respectively. The limited target area of detector determines the presence of aperture $Rect(u,v)$. As shown in Equation (1), the diffraction pattern is the convolution between free-space propagation of probe $P(u,v)$ and the spatial spectrum of object $G(u,v)$.

$$\begin{aligned} E(u,v) &= \tfrac{e^{jkz}}{j\lambda z} e^{j\frac{k}{2z}(u^2+v^2)} FFT[g(x,y)p(x,y)e^{j\frac{k}{2z}(x^2+y^2)}]Rect(u,v) \\ &= \left\{FFT[g(x,y)] * \{\tfrac{e^{jkz}}{j\lambda z} e^{j\frac{k}{2z}(u^2+v^2)} FFT[p(x,y)e^{j\frac{k}{2z}(x^2+y^2)}]\}\right\} Rect(u,v) \\ &= \{G(u,v) * P(u,v)\} Rect(u,v) \\ &= \left\{\iint G(\alpha,\beta)P(u-\alpha, v-\beta)d\alpha d\beta\right\} Rect(u,v) \end{aligned} \quad (1)$$

For ptychography, the object $g(x,y)$ is a weakly scattering object in several cases, and thus the strong lower order diffraction patterns on the recording plane are mainly decided by $P(u,v)$ and is much stronger than that of the higher order diffractions, which contain fine structural information of the object. In practical experiments, the exposure time should be short enough to avoid any saturation due to the limited dynamic range of detector. As a consequence, only very limited weak higher order diffraction patterns are recorded. Consequently, many fine structures of the sample cannot be identified in the reconstructed image. This will result in getting a poor resolution in many cases.

Figure 1(*a*) indicates the convolution operation between $P(u,v)$ and $G(u,v)$, where the integration $\int P(u-\alpha, v-\beta)G(\alpha,\beta)d\alpha d\beta$ makes the value of $G(u,v)$ at any coordinate (u,v) spreads out into a range $(u \pm W, v \pm W)$, where 2 W is the width is of $P(u,v)$, and the final diffraction patterns $E(u,v)$ is much flatter than $G(u,v)$. Figure 1(*b*) indicates the saturation taking place in the central region of diffraction pattern, and the section filled

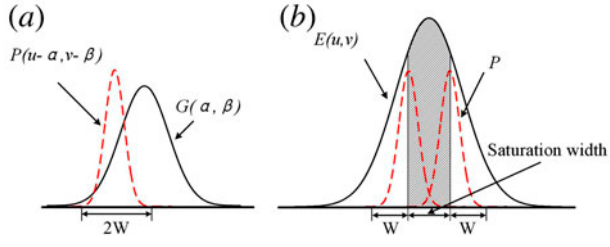

Figure 1. (*a*) The convolution between specimen spectrum $G(u,v)$ and the free-space propagation of illumination $P(u,v)$. The width of $P(u,v)$ is 2 W. (*b*) Describes the saturation in the measured data by oblique lines and indicates the case when the width of saturation is smaller than 2 W. (The colour version of this figure is included in the online version of the journal.)

with oblique line indicates the range where the saturation takes place. According to the property of convolution, if the width of saturation is smaller than 2 W, all the information of $G(u,v)$ within the saturation area can still be retrieved from the unsaturated data. In other words, the saturation in this case does not cause any information loss. With an appropriately strong illumination, the central part of diffraction will be still saturated while also making the higher order diffraction beam strong enough to be detected. Since the higher order diffraction beam corresponds to the fine structural information of object, it is possible to generate better images with ptychography using properly saturated diffraction pattern than using unsaturated diffraction patterns. To some degree, this can be a simplified model for the exclusive relevance between the whole spectrum of finite object and the segmental spectrum or mutilated diffraction pattern [29] and also can account for the success of super-resolution imaging via ptychography named SR-PIE by Maiden [27] in 2011.

Figure 2 shows the typical setup for ptychographic imaging, where the beam from a tiny hole with diameter of R is used as the illumination $P(r)$ on the sample after propagating a distance of L_1, while the specimen with complex transmission function $g(r)$ is stepped through the optical axis. The specimen is addressed by $g(r–\delta_n)$ at the nth position. The diffraction patterns recorded at the distance of L_2 behind the sample are $I_n(r)$, $n = 1…N$, respectively. The $r = [x,y]$ is coordinate vector, and $\delta_n = [\delta x,\delta y]$ is the displacement vector of specimen for the nth position. Using a properly strong illumination, the saturation will take place at the central region of diffraction pattern. According to the above analysis, the saturated diffraction patterns can be used to reconstruct better image than unsaturated patterns as we can properly extract the information from the saturated data properly. The following iterative scheme is the method used in several researches to reconstruct the probe and object functions with information lost in some part of the diffraction patterns [24–27]. The iteration starts with a suitable initial guess of specimen $g_1^1(r)$ and probe $p_1^1(r)$, and in the kth iteration:

(1) Move specimen $g_k^n(r)$ relative to probe according to displacement vector δ_n for the nth position and calculate the exit wave of specimen $\varphi_k^n = p_k^n(r)g_k^n(r-\delta_n)$ before propagating it to detector domain according to $\psi_k^n = F\langle\varphi_k^n\rangle = F\langle p_k^n(r)g_k^n(r-\delta_n)\rangle$, where F represents the propagation process.

(2) Update the calculated wave ψ_k^n by Equation (2):

$$\tilde{\psi}_k^n = \begin{cases} \sqrt{I_n(r)}\psi_k^n/|\psi_k^n| & r \notin \gamma \\ \psi_k^n & r \in \gamma \end{cases} \tag{2}$$

where γ is the set of points in the saturated section of recorded pattern $I_n(r)$.

(3) Inverse transform the updated $\tilde{\psi}_k^n$ back to specimen domain, update and obtain the new estimate of probe wave $p_k^{n+1}(r) = \tilde{p}_k^n(r)$ and specimen transmission function $\tilde{g}_k^n(r-\delta_n)$ with Wigner-filter-like update function below.

$$\tilde{g}_k^n(r-\delta_n) = g_k^n(r-\delta_n) + \beta\frac{p_k^n(r)}{|p_k^n(r)|_{\max}^2}\left(F^{-1}\langle\tilde{\psi}_k^n\rangle - \varphi_k^n\right) \tag{3}$$

$$\tilde{p}_k^n(r) = p_k^n(r) + \beta\frac{g_k^n(r-\delta_n)}{|g_k^n(r-\delta_n)|_{\max}^2}\left(F^{-1}\langle\tilde{\psi}_k^n\rangle - \varphi_k^n\right) \tag{4}$$

Inverse move $\tilde{g}_k^n(r-\delta_n)$ according to δ_n for the new estimate of specimen $g_k^{n+1}(r)$ in the next iteration for $(n+1)$th position. The factor β is a constant.

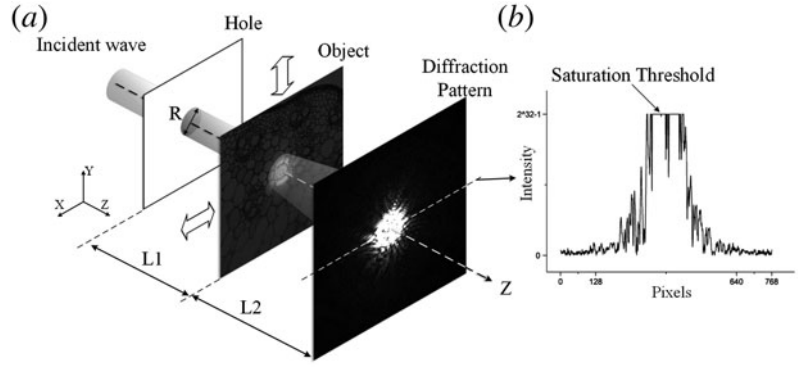

Figure 2. The typical arrangement of modified ePIE. The saturated pattern is recorded due to an incident wave with high intensity and limited dynamic range of detector. The intensity distribution along the dash line is shown in the right plot.

(4) Repeat procedure (1)–(3) for the consecutive positions from 1 to N and obtain the modified estimates of probe wave and transmission function of specimen, which could be regarded as the initial estimates for $(k+1)$th iteration.

The process above is repeated until $g_k(r)$ and $p_k(r)$ in the kth iterations have been reconstructed with adequate iterations while the lost information in $I_n(r)$ could be retrieved simultaneously.

3. Numerical simulation and performance analysis

To show the effectiveness and limitation of above reconstruction method clearly, a series of numerical simulations are carried out here. The optical arrangement is shown in Figure 2, where the incident plane wave with wavelength of 632.8 nm is transmitted through a hole of 0.5 mm and illuminates the sample after propagating to a distance of $L_1 = 25$ mm. The amplitude and phase of the object simulated are shown in Figure 3(*a*) and (*b*), respectively, and the amplitude and phase of the illumination are shown in the inset picture. One hundred diffraction patterns are recorded with a CCD of 512×512 pixels while this object is scanned in a grid of 10×10 positions. The distance between object and CCD is 40 mm and the size of each CCD pixel is $7.4 \times 7.4\ \mu m^2$. The dynamic range of CCD is assumed to be 2^8. In order to simplify the simulations, only Poisson noise, background noise, and quantization noise have been considered in the calculations to make the simulations close to the experimental reality, and the influence of CCD saturation on the reconstruction quality is evaluated with RMS error of $\mathrm{Error}(n) = \sum |g(r) - \gamma g_n(r)|^2 \Big/ \sum |g(r)|^2$ in nth iteration. The parameter γ is given by $\gamma = \sum g(r) g_n^*(r) \Big/ \sum |g_n(r)|^2$ [12,19] to eliminate the unavoidable constant scaling and phase shift in ePIE algorithm.

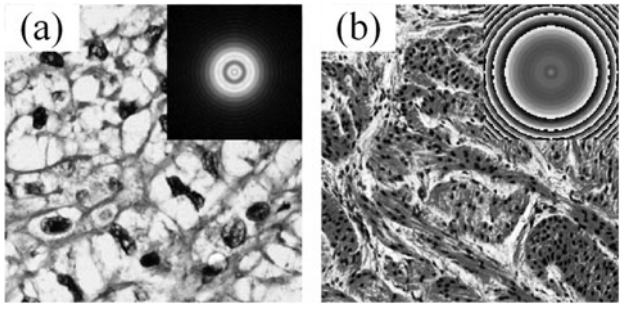

Figure 3. Amplitude (*a*) and phase (*b*) of the specimen for simulations while the corresponding amplitude and phase of illumination are shown in the up-right corner.

Figure 4(*a*) is the calculated diffraction intensity pattern with maximum value of 2^8–1 and minimum value of zero. When the intensity of illumination is six times stronger than that in Figure 4(*a*), data saturation will take place in the central part of diffraction pattern where the intensity has a value larger than 2^8–1. One frame of this kind of saturated diffraction patterns is shown in Figure 4(*d*). While comparing Figure 4(*d*) to (*a*), we can find that higher order diffractions are recorded in Figure 4(*d*). Poisson noise and extra signal

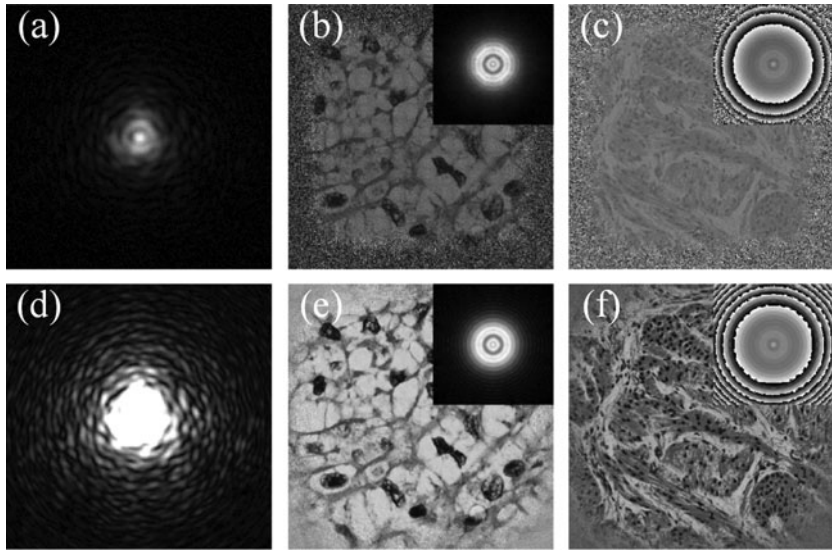

Figure 4. Unsaturated diffraction patterns (*a*), and the retrieved modulus image (*b*), and phase image (*c*), the partially saturated diffraction (*d*), and the retrieved modulus image (*e*), and phase image (*f*). The corresponding amplitude and phase of illumination are shown in the up-right corner amplitude and phase images.

randomly varying in the range 0–0.25% × (2^8–1) have been added to each pixel. The reconstructions obtained after 200 iterations are shown in Figure 4(*b*), (*c*), (*e*), and (*f*), respectively. It is obvious that the reconstructions obtained from saturated data yield much higher resolution, especially the reconstructed phase image. The final reconstruction error of Figure 4(*e*) is found to be 8.36×10^{-4}, and the final reconstruction error of Figure 4(*b*) is 1.86×10^{-2}. This result matches with the above theory very well.

According to above analysis, higher order diffraction patterns will be recorded when the strength of illumination becomes stronger. As long as the scale of the saturated area is smaller than the width of $P(u,v)$, the information lost in central saturated region can be retrieved from the outside unsaturated data. Once the scale of saturated region is larger than the width of $P(u,v)$, the information lost in the saturated region cannot be fully retrieved, and then the reconstruction quality will be degraded drastically. In other words, by slowly increasing the strength of illumination, the reconstruction should become better and better at the initial stage and then suddenly become worse. To verify this expectation, the reconstruction error changing with the increasing illumination intensity is shown in Figure 5, where α in the horizontal axis is the illumination enhancement ratio, and the vertical axis is the reconstruction error. We can find that, when α changes from 1 to 30, the reconstruction error decreases from 0.014 to 0.001 before α reaches 14. In other words, the reconstruction quality becomes 10 times better, however, when α reaches 18, the reconstruction error suddenly increases to 0.06. According to above analysis, this is due to the size of saturation region exceeds the width of $P(u,v)$ at $\alpha = 18$ and the information cannot be fully recovered anymore. In Figure 5, the inserts are the corresponding diffraction patters with saturations.

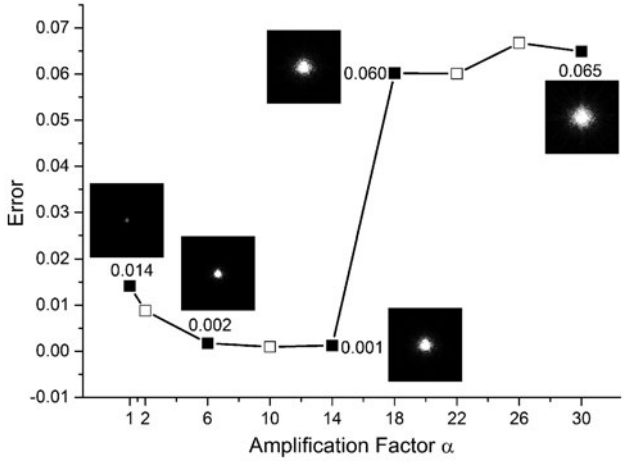

Figure 5. The reconstruction errors of differently saturated diffraction patterns.

The robustness of the method against noise is also investigated numerically. Figure 6(*a*) shows that the change in error (RMS) with the increasing noise level when saturated and unsaturated diffraction patterns are used for calculations. Figure 6(*b*) shows another comparison of error with the quantization noise.

To calculate Figure 6(*a*), different levels of background noise including Poisson noise and random noise were added to the calculated intensity. We find that, with increasing noise level, the reconstructed image always becomes worse for both reconstructions using saturated as well as unsaturated data. The reconstruction error with partially saturated data ($\alpha = 6$) is always much smaller than that of the saturated data when the background noise ratio varies from 0.125 to 4%. The same tendency

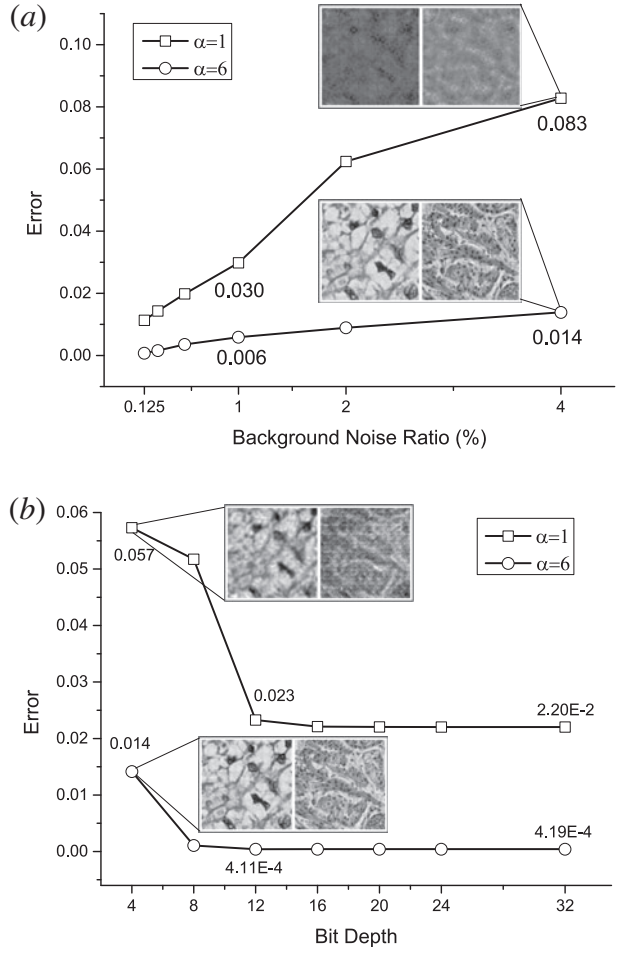

Figure 6. (*a*) Reconstruction errors changing with the increasing background noise level while saturated data and unsaturated dataset are used. (*b*) Reconstruction errors changing with different bit depth of the detector. The insets are corresponding distributions of retrieved amplitude (left column) and phase (right column) in each figure.

can also be found in the numerical simulations on the detector bit depths as shown in Figure 6(*b*). That is, while the reconstructed image always becomes better with increasing bit depth, the reconstruction with saturated data is always much better than that with unsaturated data. The simulation results in Figure 6 demonstrate the practicability of the proposed method for real experiments.

4. Experiments and results

We have performed experiments to validate the described reconstruction method with saturated data. The wavelength of illumination λ is 632.8 nm, and the aperture diameter R is 0.7 mm. An 8 bits Pike-F421B CCD with pixels of 2048 × 2048 on a 7.4 μm pitch is used to record the diffractions. A dataset of 100 diffraction patterns is recorded by automatic control system in ten minutes while the specimen, which is a cucurbit stem mounted on a stage moves in a grid of 10 × 10 different positions. Figure 7(*a*) shows one of the unsaturated diffractions, and Figure 7(*f*) and (*k*) are, respectively, the reconstructed modulus and phase images. Since the presence of higher order diffractions is quite less in the recorded pattern, the resolution of reconstructed images is not high, and hence, the structure of each individual cell cannot be identified. By increasing the strength of illumination 1.2 times, a slightly saturated diffraction pattern is obtained which is shown in Figure 7(*b*). In comparison with the images reconstructed with unsaturated data, the resolution is improved obviously due to an increase in the presence of higher order diffractions as evidenced by the reconstructed modulus image Figure 7(*g*), and the reconstructed phase image Figure 7(*l*). Increasing the strength of illumination further, by 5 times, the diffraction pattern obtained is shown in Figure 7(*c*) which records more higher order diffractions. The reconstructed modulus image Figure 7(*h*) and phase image Figure 7(*m*) are having more details, and the structure of each individual cell can be clearly identified. However, by further increasing the strength of illumination to 10 times, though more high-order diffractions are recorded in Figure 7(*d*), the reconstructed modulus image Figure 7(*i*) and phase image Figure 7(*n*) become blurred. According to the above analysis, this happened because the saturation area is larger than the width of $P(u,v)$. Increasing the strength of illumination further results in diffraction pattern as shown in Figure 7(*e*). The respective modulus and phase images, Figure 7(*j*) and (*o*), indicate that the reconstruction quality is seriously degraded, and almost no structure of the specimen can be identified.

We repeated the above experiment using a resolution test target (USAF 1951) to evaluate the resolution

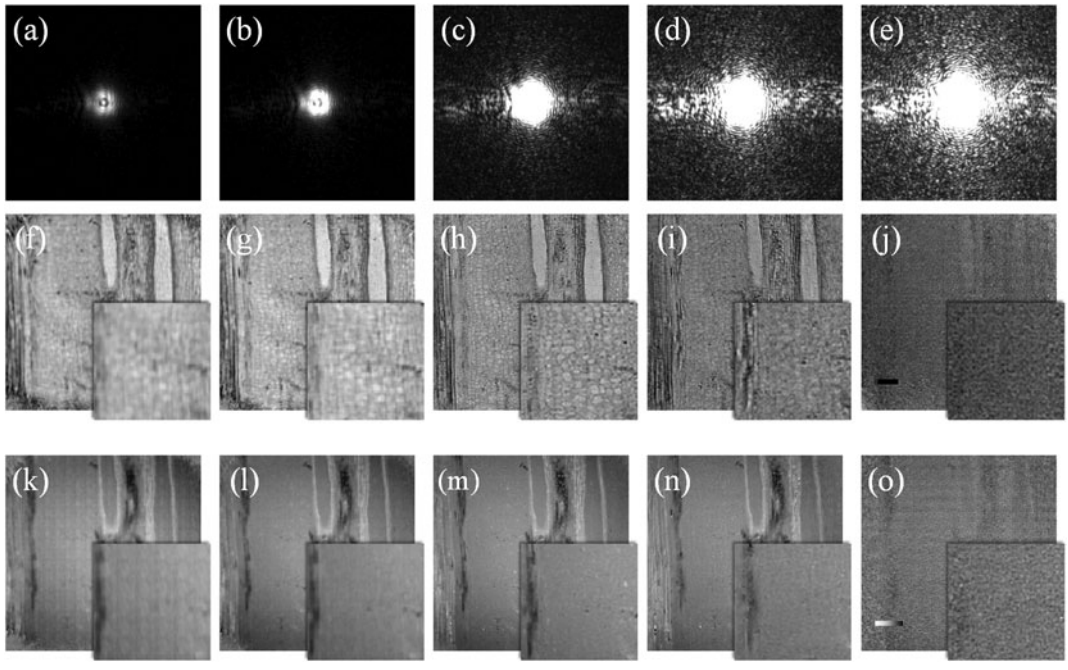

Figure 7. Reconstructed images from diffraction patterns obtained with illuminations of different strength. The first row shows a set of recorded diffraction patterns, and the second and third rows show the corresponding reconstructed amplitude and phase distributions obtained after 200 iterations. The central bright region in each diffraction pattern in the first row indicates the saturation. The scale bar is 200 μm in the second row and $-\pi$ to π in the third row.

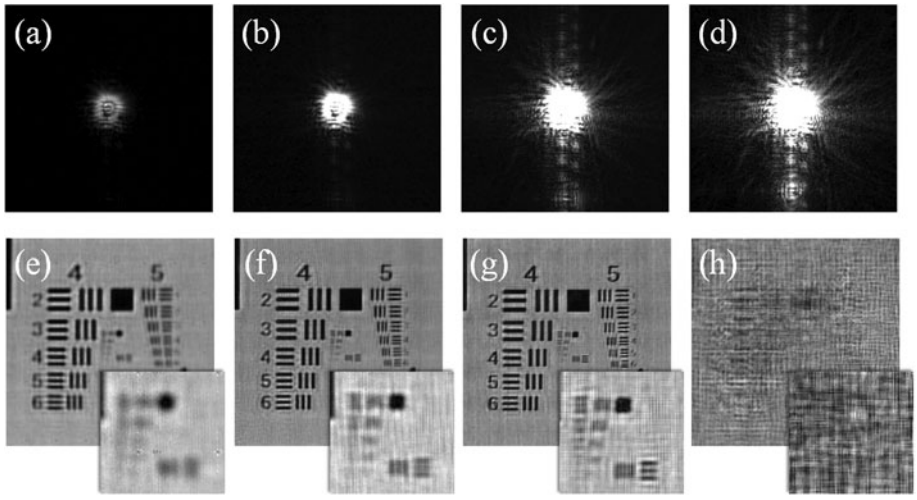

Figure 8. Reconstructions of resolution test target with differently saturated datasets. The first row is the recorded diffraction patterns of different illumination strength, and the corresponding reconstructions are shown in the second row. The inset in the right-down corner is the zoomed-in view of the group 6 of test target.

improvement quantitatively. Figure 8(*a*)–(*d*) are the recorded diffraction patterns with the strength of the illumination increased by twofold in each case. As seen earlier, higher order diffractions are recorded with stronger illuminations. Figure 8(*e*)–(*h*) are the corresponding reconstructed modulus images, and we can find that Figure 8(*g*) has the highest resolution of about 71.84 pair lines/mm (element 2 of group 6). Compared to Figure 8(*e*), which has a resolution of 45.25 pair lines/mm (element 4 of group 5), the resolution in Figure 8(*g*) is improved by 1.6 times. As the illumination strength is increased by eight times, the resolution degrades seriously and almost no structural information can be identified from the reconstruction. The reason is because the saturation area is larger than the width of $P(u,v)$, and hence the lost information in the saturated region cannot be fully recovered with Ptychography.

5. Discussion and conclusion

Neglecting the intensity constraint within the saturation area with inaccurate intensity, information can be an effective method to compensate the information lost due to the occurrence of saturation on the recording plane. This is possible due to the convolution effect between the illumination and the object functions. The lost information within the saturated region can be retrieved from the unsaturated region as long as the area of the saturated region is smaller than the scale of $P(u,v)$. However, once the saturated region exceeds this size, the reconstruction quality will degrade seriously since the lost information cannot be fully retrieved. It is demonstrated experimentally that by properly selecting the illuminating strength and accordingly optimizing the size of saturated area, the resolution can be easily improved by 1.6 times in our experiments. Though the main discussion is focused on the saturation of diffraction, the concept can also be extended to reconstructions with central diffractions blocked with minimum modifications.

Disclosure statement

No potential conflict of interest was reported by the authors.

Funding

This work was supported by the One Hundred Persons' Project of Chinese Academy of Sciences [grant number 1104331-JR0] and funding of GFZX0205010502.12.

References

[1] Nobuo, T. *Sci. Technol. Adv. Mater.* **2008,** *9,* 014111-1–014111-11.
[2] Latychevskaia, T.; Longchamp, J.-N.; Fink, H.-W. *Opt. Express* **2012,** *20,* 28871–28892.
[3] Hoppe, W. *Acta Crystallogr.* **1969,** *A25,* 495–501.
[4] Hoppe, W.; Strube, G. *Acta Crystallogr.* **1969,** *A25,* 502–507.
[5] Hoppe, W. *Acta Crystallogr.* **1969,** *A25,* 508–514.
[6] Gerchberg, R. *Optik* **1972,** *35,* 237–246.
[7] Fienup, J.R. *Appl. Opt.* **1982,** *21,* 2758–2769.
[8] Fienup, J.R.; Kowalczyk, A.M. *J. Opt. Soc. Am. A.* **1990,** *A7,* 450–458.
[9] Nellist, P.D.; McCallum, B.C.; Rodenburg, J.M. *Nature.* **1995,** *374,* 630–632.
[10] Chapman, H.N. *Nat. Mater.* **2009,** *8,* 299–301.
[11] Miao, J.; Charalambous, P.; Kirz, J.; Sayre, D. *Nature.* **1999,** *400,* 342–344.
[12] Zuo, J.M.; Vartanyants, I.; Gao, M.; Zhang, R.; Nagahara, L.A. *Science.* **2003,** *300,* 1419–1421.

[13] Rodenburg, J.M. *Adv. Imaging Electron.* **2008,** *150,* 87–184.
[14] Fienup, J.R.; Wackerman, C.C. *J. Opt. Soc. Am. A.* **1986,** *A3,* 1897–1907.
[15] Fienup, J.R. *J. Opt. Soc. Am. A.* **1987,** *A4,* 118–123.
[16] Rodenburg, J.M.; Faulkner, H.M.L. *Appl. Phys. Lett.* **2004,** *85,* 4795–4797.
[17] Humphry, M.J.; Kraus, B.; Hurst, A.C.; Maiden, A.M.; Rodenburg, J.M. *Nat. Commun.* **2012,** *3,* 730-1–730-7.
[18] Rodenburg, J.; Hurst, A.; Cullis, A.; Dobson, B.; Pfeiffer, F.; Bunk, O.; David, C.; Jefimovs, K.; Johnson, I. *Phys. Rev. Lett.* **2007,** *98,* 034801-1–034801-4.
[19] Maiden, A.M.; Rodenburg, J.M. *Ultramicroscopy* **2009,** *109,* 1256–1262.
[20] Rodenburg, J.M.; Hurst, A.C.; Cullis, A.G. *Ultramicroscopy* **2007,** *107,* 227–231.
[21] Wang, H.; Liu, C.; He, X.; Pan, X.; Zhou, S.; Wu, R.; Zhu, J. *High Power Laser Sci. Eng.* **2014,** *2,* e25-1–e25-14.
[22] Zhang, F.; Peterson, I.; Vila-Comamala, J.; Diaz, A.; Berenguer, F.; Bean, R.; Chen, B.; Menzel, A.; Robinson, I.K.; Rodenburg, J.M. *Opt. Express* **2013,** *21,* 13592–13606.
[23] Maiden, A.M.; Humphry, M.J.; Sarahan, M.C.; Kraus, B.; Rodenburg, J.M. *Ultramicroscopy* **2012,** *120,* 64–72.
[24] Maiden, A.M.; Morrison, G.R.; Kaulich, B.; Gianoncelli, A.; Rodenburg, J.M. *Nat. Commun.* **2013,** *4,* 1669.
[25] Vila-Comamala, J.; Diaz, A.; Guizar-Sicairos, M.; Mantion, A.; Kewish, C.M.; Menzel, A.; Bunk, O.; David, C. *Opt. Express* **2011,** *19,* 21333–21344.
[26] Thibault, P.; Dierolf, M.; Menzel, A.; Bunk, O.; David, C.; Pfeiffer, F. *Science* **2008,** *321,* 379–382.
[27] Maiden, A.M.; Humphry, M.J.; Zhang, F.; Rodenburg, J.M. *J. Opt. Soc. Am. A.* **2011,** *A28,* 604–612.
[28] Liu, H.; Xu, Z.; Zhang, X.; Wu, Y.; Guo, Z.; Tai, R. *Appl. Opt.* **2013,** *52,* 2416–2427.
[29] Gerchberg, R. *J. Mod. Opt.* **1974,** *21,* 709–720.